

Physics of Solid and Liquid Alkali Halide Surfaces Near the Melting Point

T. Zykova-Timan,¹ D. Ceresoli,¹ U. Tartaglino,^{1,2} and E. Tosatti^{1,3}

¹*International School for Advanced Studies (SISSA),
and INFN DEMOCRITOS National Simulation Center,
via Beirut 2-4, I-34014 Trieste, Italy*

²*IFF, FZ-Jülich, 52425 Jülich, Germany*

³*International Centre for Theoretical Physics (ICTP), P.O.Box 586, I-34014 Trieste, Italy*

This paper presents a broad theoretical and simulation study of the high temperature behavior of crystalline alkali halide surfaces typified by NaCl(100), of the liquid NaCl surface near freezing, and of the very unusual partial wetting of the solid surface by the melt. Simulations are conducted using two-body rigid ion BMHFT potentials, with full treatment of long-range Coulomb forces. After a preliminary check of the description of bulk NaCl provided by these potentials, which seems generally good even at the melting point, we carry out a new investigation of solid and liquid surfaces. Solid NaCl(100) is found in this model to be very anharmonic and yet exceptionally stable when hot. It is predicted by a thermodynamic integration calculation of the surface free energy that NaCl(100) should be a well ordered, non-melting surface, metastable even well above the melting point. By contrast, the simulated liquid NaCl surface is found to exhibit large thermal fluctuations and no layering order. In spite of that, it is shown to possess a relatively large surface free energy. The latter is traced to a surface entropy deficit, reflecting some kind of surface short range order. Finally, the solid-liquid interface free energy is derived through Young's equation from direct simulation of partial wetting of NaCl(100) by a liquid droplet. It is concluded that three elements, namely the exceptional anharmonic stability of the solid (100) surface, the molecular short range order at the liquid surface, and the costly solid liquid interface, all conspire to cause the anomalously poor wetting of the (100) surface by its own melt in the BMHFT model of NaCl – and most likely also in real alkali halide surfaces.

PACS numbers: 68.35.Rh, 68.35.Md, 68.45.Gd, 82.65.Dp, 68.10.Cr, 61.50.Jr

I. INTRODUCTION

Attention is increasing toward adhesion and wetting, the structure and physics of solid-liquid interfaces especially at high temperatures, and the structure of liquid surfaces, particularly of complex and molecular systems. In order to gain more insight into these problems, there is a strong need for good case studies, to use as well-understood starting points.

One easy starting point is to study the contact of a liquid with *its own* solid, a clear situation where there will be no ambiguity of physical description, no uncertainty in chemical composition, no segregation phenomena, all of them complications present in the study of contact between different substances. Contact of a liquid with the surface of its own solid usually materializes spontaneously at high temperature. Most solid surfaces are known to wet themselves spontaneously with an atomically thin film of melt, when their temperature T is brought close enough to the melting point T_m of the solid. The phenomenon whereby the thickness $l(T)$ of the liquid film diverges continuously (and critically) as $T \rightarrow T_m$, is commonly referred to as (complete) surface melting [1, 2].

Surface melting is indeed a very natural thing to happen, because it corresponds to complete wetting of a solid substrate by the same identical substance, only in liquid form. Another name for surface melting, better suited for the fluid community [3, 4], could be complete interfacial wetting. Due to surface melting, a solid with free

surfaces cannot generally be overheated above its thermodynamical bulk T_m . The free energy barrier for the passage from solid to liquid generally requires nucleation and implies hysteresis. Although this is not generally observable for reasons exposed below, it should be theoretically possible to overheat a solid, at least insofar as one can exclude the presence of defects that could act as nucleation centers.

In the melting phase transition, the solid surface itself represents a (nearly) ubiquitous defect that continuously nucleates the liquid, thus usually preventing overheating of the solid. A generic crystal surface simply does not remain solid at high temperature, and spontaneously wets itself with a liquid film of increasing thickness very close to the melting point. The thermodynamical condition for surface melting, or complete interfacial wetting, to occur, is that the solid-vapor (SV) interface should turn itself spontaneously into the solid-liquid (SL) plus liquid-vapor (LV) interface pair, or:

$$\gamma_{SV} = \gamma_{SL} + \gamma_{LV}, \quad (1)$$

where the γ 's are interface free energies at the triple point.

There are a number of known exceptions to this behavior. On some solid surfaces the liquid film does begin to form upon heating, but its thickness levels off to a finite value instead of diverging as $T \rightarrow T_m$ (so-called blocked or incomplete [5] surface melting). More remarkably, some other solid surfaces remain dry and fully crystalline up to the bulk triple point. This *surface non-*

melting phenomenon, originally discovered in molecular dynamics simulations of Au(111) [6] and independently observed experimentally in Pb(111) [7], takes place at the close-packed faces of several metals, such as Al(111) [8].

Thermodynamically, surface non-melting will occur if there is a free energy loss in converting the SV interface into the SL plus LV interfaces pair, namely

$$\gamma_{SV} < \gamma_{SL} + \gamma_{LV}. \quad (2)$$

In that case, the liquid will wet the solid at best *incompletely*. A liquid droplet deposited in full equilibrium on the solid surface will not spontaneously spread. It will settle instead in a metastable partial wetting geometry such as that of Fig. 1. The metastable droplet is characterized by two angles θ_{SL}, θ_{LV} , and by two curvature radii (not shown) R_{SL}, R_{LV} of the solid-liquid and liquid-vapor interfaces, approximately obeying the generalized Young equations [9]:

$$\gamma_{SV} = \gamma_{SL} \cos \theta_{SL} + \gamma_{LV} \cos \theta_{LV} \quad (3)$$

$$R_{LV} \sin \theta_{LV} = R_{SL} \sin \theta_{SL} \quad (4)$$

The temporary settling of a metastable liquid droplet on the surface of the same solid substance, schematically depicted in Fig. 1 and discussed by Nozières [9], was demonstrated in simulation in Ref. [10] for Al/Al(111), but not verified experimentally yet [11].

Here we wish to move on from elemental to molecular systems. Alkali halides are our natural prototype choice, because they represent a well defined class of substances whose liquids do not wet their own solid, and because they have otherwise long been studied experimentally and theoretically. Molten salts and their surfaces were extensively investigated by macroscopic techniques [12]. A partial wetting angle $\theta_{LV} = 48^\circ$ is known for liquid NaCl on NaCl(100) at the melting point $T_m = 1074$ K (and similar results also hold for other alkali halides) [13, 14]. Such a large angle underlines a strikingly poor wetting of the liquid onto its own solid, large by comparison with other known cases. For example, $\theta_{LV} \sim 15^\circ$ is observed for liquid Pb/Pb(111) [15], or $\sim 19^\circ$ is obtained by simulation of Au/Au(111) [10]. Should liquid surface layering be, as was the case in metals, the culprit in NaCl too, the layering magnitude and its effect should indeed be exceptionally strong, and amenable to experimental verification. Several simulations on alkali halide liquids suggest instead that there is no layering whatsoever [16, 17]. A second possible mechanism leading to surface non-melting may arise from van der Waals forces. Whenever the melt is optically more dense than the solid, the so-called Hamaker constant H governing the effective SL-LV interface interaction H/l^2 may turn negative. The resulting attraction impedes complete melting, as is the case for valence semiconductors such as silicon [2]. However, liquid NaCl is 26% less dense than the solid, and here the Hamaker constant is certainly positive [18].

That leaves the question of explaining the exceptionally poor wetting of NaCl(100) by liquid NaCl completely

open. In order to shed light on this question and on the underlying physics, we undertook extensive simulation studies of the molten NaCl surface, and also of the NaCl(100) solid surface, at and close to the melting point.

The plan of the rest of this paper is as follows. We will introduce first the simulation methods and the potentials used. Subsequently we will proceed to a careful characterization of all bulk properties of this model. The bulk solid and the bulk liquid will be simulated, and the results compared to experimental data and to previous theory and simulations. The bulk zero-pressure melting temperature, very close to the triple point temperature, will be extracted for this model potential by direct simulation of the solid-liquid coexistence. Next, extensive slab simulations will be used to obtain a quantitative description of the solid (100) surface near and above bulk melting, and of the liquid surface in the same temperature range. The solid surface free energy γ_{SV} will be calculated by thermodynamic integration. That of the liquid surface γ_{LV} will be calculated by means of the Kirkwood-Buff virial formula. The two will be compared and discussed. An effective harmonic calculation will be implemented showing the importance of anharmonicity in stabilizing the high temperature solid surface. A modified calculation of the liquid surface free energy will be introduced to understand the poor temperature dependence of γ_{LV} , eventually explained in terms of surface short range order. Finally the solid-liquid interface free energy γ_{SL} will be calculated via Young's equation from a direct simulation of partial wetting of a liquid droplet on the solid surface at the melting point. The resulting large value of γ_{SL} is connected to the large density jump. In the concluding discussion, it is argued that all three separate physical mechanisms that conspire to give rise to poor wetting, by lowering γ_{SV} and simultaneously raising γ_{LV} and γ_{SL} eventually stem from charge order and charge neutrality of this ionic system.

II. HAMILTONIAN, AND SIMULATION METHOD

NaCl was modeled by the classic pairwise Born-Mayer-Huggins-Fumi-Tosi (BMHFT) rigid ion potential [19]:

$$V(r_{ij}) = \frac{Z_\alpha Z_\beta}{r_{ij}} + A_{\alpha\beta} \exp(-Br_{ij}) - \frac{C_{\alpha\beta}}{r_{ij}^6} - \frac{D_{\alpha\beta}}{r_{ij}^8}. \quad (5)$$

Here α and β stand for either + or -, Z_α and Z_β are the ionic charges (+1 for *Na* and -1 for *Cl*), the first term is the Coulomb interaction energy, the second is the short-range Pauli repulsion, and last two terms are induced dipole-dipole and dipole-quadrupole van der Waals interactions. The values of the parameters are reported in Table II.

Polarization forces [17], though not negligible for the quantitative description of molecules, low-density ionic fluids, and other properties, do not appear to be crucial in the present context. They are neglected in order to

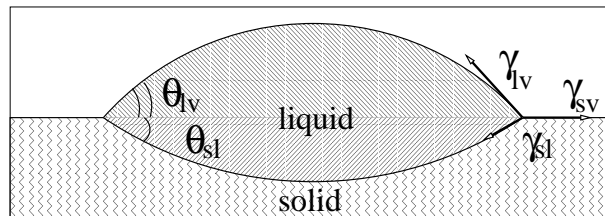


FIG. 1: Sketch of the liquid drop partially wetting its own solid, showing the balance of the forces acting at the interfaces.

	Na-Na	Cl-Cl	Na-Cl
A (eV)	424.097	3488.998	1256.31
B (\AA^{-1})	3.1545	3.1545	3.1545
C (eV \AA^6)	1.05	72.5	7.0
D (eV \AA^8)	0.499	145.427	8.676

TABLE I: Parameters of Born-Mayer-Huggins-Fumi-Tosi potential for NaCl.

concentrate on the BMHFT model, whose greater simplicity allows a much more extensive computational exploration of the wetting properties [20].

Bulk systems were studied at constant volume with cubic simulation cells comprising up to 10000, but more typically 3000÷5000, NaCl molecular units. Surfaces were studied with periodically repeated slabs – consisting of 12 ÷ 24 planes – separated by about 80 \AA of vacuum. The long range Coulomb interaction between ions was treated in full. We implemented a 3D Ewald summation with repeated slabs and periodic boundary conditions along the direction z orthogonal to the surfaces as well as parallel to the (x, y) surface plane. The alternative choice of a single slab with 2D Ewald summation, physically more natural, was discarded as computationally more demanding [21]. In our repeated slab 3D Ewald scheme, the large vacuum thickness is required in order to reduce spurious electrostatic couplings of instantaneous fluctuating dipoles in liquid surfaces facing one another across the vacuum gap. Moreover, the Ewald sums were carried out for better convergence with conducting (“tin foil”) boundary conditions in the in-plane directions and with insulating or vacuum boundary conditions in the direction normal to the surface (see Ref. [21]). We performed both microcanonical and canonical simulations. In canonical runs, temperature was controlled by velocity-rescaling. Despite the size and time limitations imposed by long range forces, great care was taken to run simulations long enough for a clear equilibration, typically 100÷300 ps at T_m , but longer when required. Finally, in all simulations involving the solid, whether as a bulk crystal, or at solid-liquid coexistence, or as a solid slab, we adjusted the cell size at each temperature so as to enforce the theoretical equilibrium lattice parameter independently computed as the one that gave a vanishing bulk stress (see Sec. III A).

III. BULK PROPERTIES

A. Bulk Solid NaCl

First of all, we verified how faithfully the bulk properties of solid and liquid NaCl are reproduced by the BMHFT potentials. Thermal expansion of the solid is dictated by the increase of equilibrium lattice spacing at zero pressure as a function of temperature. We performed several simulations at constant temperature and volume, and computed the equilibrium lattice spacing by seeking the cell size that yielded vanishing pressure at each given temperature. The overall interpolated result is shown in Fig. 2, where it is compared with experimental data from various sources [22]. The temperature dependent cell size obtained in this manner was subsequently enforced in all subsequent simulations involving solid NaCl, as mentioned earlier. The 298 K calculated equilibrium lattice spacing and linear expansion coefficient $\alpha = (3V)^{-1}dV/dT$ were 5.683 \AA and $40.5 \cdot 10^{-6} \text{ K}^{-1}$ respectively (5.635 \AA and $38.3 \cdot 10^{-6} \text{ K}^{-1}$ are the experimental values [22]).

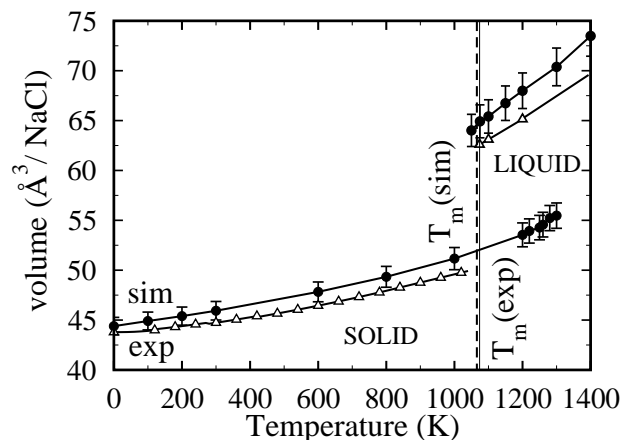


FIG. 2: NaCl volume expansion vs temperature. Both the theoretical (filled circles) melting temperature and change of the volume at T_m are very similar to the experimental ones (empty triangles).

At higher temperature, notably above 600 K, the anharmonicity is seen to get stronger, and expansion becomes somewhat nonlinear. It should be noted that our procedure continues to work, and is in fact very accurate

at these higher temperatures. The simulated bulk solid remains locally stable and does not spontaneously melt (at least for our cell sizes and for times within 200 ps) until a maximum temperature $T_s \sim 1305$ K. This maximum bulk metastability temperature, necessarily higher than the ordinary melting temperature T_m , approximates the “spinodal” temperature of bulk NaCl, defined as the point where the solid phase ceases to be a local free energy minimum (for example by losing its mechanical stability). As we will see further below, this bulk spinodal temperature is indeed predicted well above the melting temperature, precisely $T_s \sim T_m + 240$ K in the BMHFT model. It would be interesting to check this prediction by studying, e.g., spontaneous nucleation of the liquid inside the solid, locally heated by for example two crossed laser beams.

Root mean square displacements $(\overline{\Delta r^2})^{1/2}$ (RMSD) of Na^+ and Cl^- ions were extracted from the high temperature bulk NaCl solid simulations. As shown in Fig. 3 the value at 1066 K is 0.61 Å for Na and 0.59 Å for Cl, comparable with experimental estimates of 0.5 Å and 0.48 Å at the melting point [23]. The corresponding calculated Lindemann ratios at 1066 K $\delta = (\overline{\Delta r^2})^{1/2}/a$, (a is the interatomic distance) are 20% and 22%, compared with experimental estimates at T_m obtained from Debye-Waller factors of 17% and 20% [23]. Simulation appears to slightly overestimate the thermal vibration amplitudes, but we note that the uncertainties in the experimental procedure where RMSDs were extracted seem much larger than this discrepancy. In any case the RMSD values are very much larger than the typical values between 10% and 14% of the Lindemann ratio for most solids at T_m . This large overshoot of the alkali halide bulk Lindemann ratios can be rationalized by noting that whereas large thermal vibrations may very effectively destabilize atoms inside its bulk solid cage when interatomic forces are short ranged, they will much less effectively do so when forces are long range as is the case in strongly ionic solids. Simulations show that high temperature NaCl is in the BMHFT model a strongly vibrating, strongly anharmonic, and yet unusually stable solid. As we shall show later, the same is true of the NaCl(100) surface.

The vibrational spectral properties of warm NaCl can also be easily extracted, for later use, by Fourier transforming the velocity-velocity correlation functions:

$$V_{\text{Na}}(\omega) = \frac{1}{2\pi} \int_0^\infty dt e^{i\omega t} \langle \mathbf{v}_{\text{Na}}(t) \cdot \mathbf{v}_{\text{Na}}(0) \rangle, \quad (6)$$

and similarly for Cl. The two spectral densities $V_{\text{Na}}(\omega)$ and $V_{\text{Cl}}(\omega)$ extracted at 300 K and at 1066 K are shown in the Fig. 4.

Generally, we note that our simulated vibrational spectra do not compare well in the details – even if not unreasonably in their gross features – with the more realistic spectral densities of Ref. [24] taken from the literature, and corresponding to very accurate shell model fits to experimental phonon spectra (Fig. 5). The rigid ion model is notoriously too crude to reproduce fine features as the

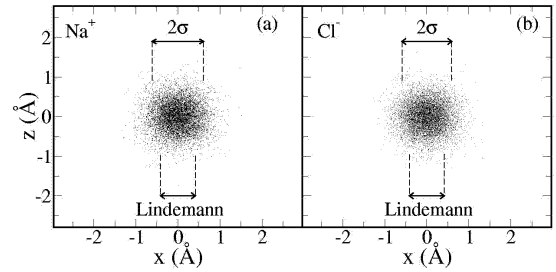


FIG. 3: The instantaneous displacements of the Na^+ (a) and Cl^- (b) ions in simulated bulk NaCl at 1066 K (bulk melting point of the Tosi-Fumi model). The displacement distributions are well fit by gaussian distributions whose widths are indicated. The much smaller widths predicted by the Lindemann melting criterion $(\overline{\Delta r^2})^{1/2} \sim 0.14 \times a$, where a is the interatomic distance, are also shown.

detailed vibrational spectra, heavily affected by non rigid ion effects [25]. Nonetheless it is not unreasonable to believe that the overall temperature evolution of spectral densities can still be taken as representative of the real situation. The high temperature spectra show a considerable anharmonic softening and broadening relative to the room temperature ones.

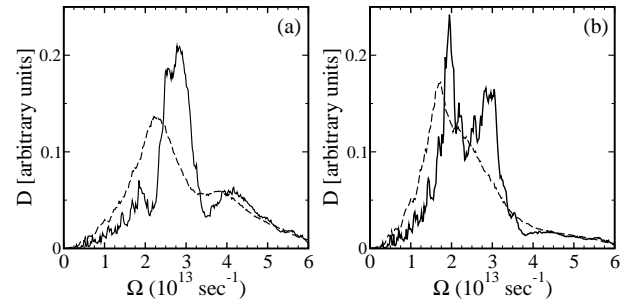


FIG. 4: Vibrational density of states of bulk solid NaCl for (a) Na^+ and (b) Cl^- ions. Comparison between 300 K (solid line) and 1000 K (dashed line) indicates a considerable vibrational softening.

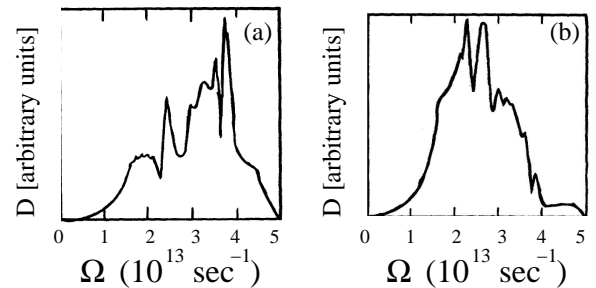


FIG. 5: Vibrational density of states of solid NaCl at low temperatures projected on (a) Na^+ and (b) Cl^- ions. From Ref. [24]

B. Bulk Liquid NaCl

Simulations of bulk liquid NaCl were conducted in close analogy to those of solid NaCl. In particular, the cell volume was adjusted isotropically to ensure vanishing pressure at every temperature. Our overall description of the liquid is very similar to that provided by many long-standing studies [26, 27, 28, 29]. The calculated liquid molecular volume is shown along with experimental values in Fig. 2. The calculated volume expansion of 27% at melting compares very well with 26% from experiment. The internal structure of the liquid, notably the Na-Cl, Na-Na and Cl-Cl radial distribution functions:

$$g(r) = \rho^{-1} \left\langle \sum_{ij} \delta(\mathbf{r} - \mathbf{R}_{ij}) \right\rangle, \quad (7)$$

quantities that are long well known, are well reproduced (Fig. 6) by the simulation. They exhibit the charge correlation typical of molten salts, the first peak of $g_{+-}(r)$ giving a typical Na-Cl distance in the liquid of 2.6 Å, about 10% shorter than in the solid.

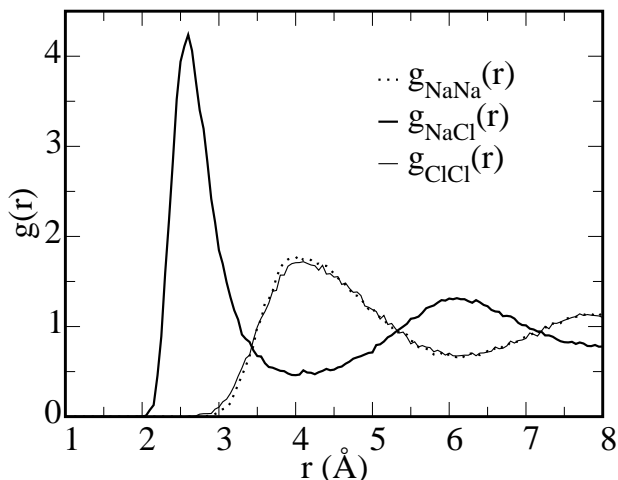


FIG. 6: The partial radial distribution functions at $T_m = 1066$ K.

From the pair correlation functions, we may calculate the bulk liquid coordination number:

$$N_{\pm} = \rho \int_0^{r_m} 4\pi r^2 g_{+-}(r) dr, \quad (8)$$

where the upper integration limit corresponds to the first local $g_{+-}(r)$ minimum, $r_m = 4.0$ Å. We find a coordination number $N = 4.6$ in liquid NaCl at 1066 K, to be compared with the much higher $N = 6$ coordination in the defect-free bulk solid. Experimental estimates of the liquid coordination number vary in a broad range from $N = 4.7$ [28] to $N = 5.8$ [29]. According to our simulation an ion in the liquid is surrounded by a cage consisting of only 4.6 ions of the opposite charge, albeit considerably

closer than in the solid. In order to better understand the nature of the effective ion cage in the liquid we studied the Na-Cl-Na and Cl-Na-Cl angular distribution in the bulk liquid:

$$P(\theta) = \left\langle \sum_{ijk} \delta\left(\theta - \arccos \frac{\mathbf{R}_{ji} \cdot \mathbf{R}_{jk}}{|\mathbf{R}_{ji}| |\mathbf{R}_{jk}|}\right) \right\rangle, \quad (9)$$

where $|\mathbf{R}_{ij}|, |\mathbf{R}_{jk}| < r_m$. The result shown in Fig. 7 exhibits a main peak at 90° and only a weaker shoulder around 150° . Similar results had been obtained by Amini [30]. The dominant 90° peak indicates in particular that the local ionic cage surrounding an ion of the opposite charge is, even in the liquid, still roughly cubic, or more precisely octahedral, as in the solid. The octahedral cage linear size is smaller by about 10% than that of the solid. The 4.6 surrounding ions are distributed on the 6 corners of this cage, which therefore contains on average about 1.4 vacancies.

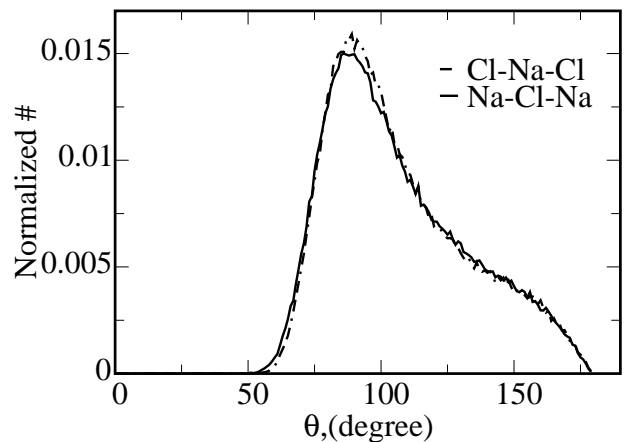


FIG. 7: The angular distribution function of simulated liquid NaCl at T_m .

The diffusion coefficient:

$$D = \lim_{t \rightarrow \infty} \frac{1}{6t} \left\langle \sum_i |\mathbf{R}_i(t) - \mathbf{R}_i(0)|^2 \right\rangle, \quad (10)$$

was also computed during simulations in order to check the general quality of description of the liquid. We found $D = 10.53 \cdot 10^{-5} \text{ cm}^2/\text{s}$ at $T = 1300$ K, which compares well with experimental values like $D = 8.6 \cdot 10^{-5} \text{ cm}^2/\text{s}$ at $T = 1121$ K [31], as well as with those from previous MD simulations, such as $D = 9.5 \cdot 10^{-5} \text{ cm}^2/\text{s}$ at $T = 1267$ K [27].

Based on all the above we conclude that the BMHFT potential description of bulk liquid NaCl is on the whole very good.

C. Bulk Melting Temperature

The melting temperature of the BMHFT model of bulk NaCl is obtained directly from simulations of solid-liquid

coexistence at zero pressure [32]. At constant temperature, the interface in a bulk system which is roughly half solid and half melted (actually there are two SL interfaces because of periodic boundary conditions) will drift with simulation time one way or the other so long as the system is away from the melting temperature T_m , and will only remain stationary at $T = T_m$. At constant energy, the average temperature $\langle T \rangle$ will instead slowly drift toward the melting temperature T_m [33, 34].

We started with a crystalline bulk made up of 2880 molecular units, a geometry comprising $6 \times 6 \times 20$ conventional 4-molecule cubic NaCl cells along (x, y, z) respectively. Periodic boundary conditions (PBC) were assumed in all directions, and the volume was constant during each simulation. However, the cell size was adjusted with temperature, so as to enforce zero stress at each temperature, as detailed below. After equilibration in proximity of the presumed melting point ($T \approx 1100$ K) about one half of the 20 layers were melted by bringing them selectively at a higher temperature, while the remaining atoms in the solid phase are kept fixed on their positions. The liquid and the solid halves initially out of equilibrium were subsequently let evolve to their mutual equilibrium. The in-plane cell size, and with it the in-plane solid lattice spacing were kept fixed at their solid equilibrium value previously established for that temperature as shown in Fig. 2 of Subsec. III A. The linear cell size in the z -direction perpendicular to the solid-liquid interfaces was subsequently adjusted after each equilibration so as to cancel the uniaxial stress normal to the interfaces, compensating in particular the solid-liquid volume expansion. When the system was finally equilibrated by means of canonical MD runs (see Fig. 8), we observed the anticipated drift of the solid-liquid interfaces in opposite directions at 1050 K and 1070 K, indicating that the melting temperature must fall in between (Fig. 9a).

To sharpen up our estimate of T_m we then carried out delicately selected microcanonical simulation runs between $E = -7.2$ and -7.25 eV/molecule. Our final result was $T_m = 1066 \pm 20$ K (Fig. 9b). The conservatively large error bar quoted is mainly due to a residual pressure uncertainty of ~ 0.5 kbar. The real uncertainty is probably smaller, since we also found later that systems with free surfaces, and thus with a pressure more accurately close to zero, melt in bulk within 5 K of 1066 K. We also estimate that the error of T_m due to other factors, including small system size, and fluctuations, to be smaller than 20 K. For instance, the melting temperature of an unrealistically small system made of $6 \times 6 \times 4$ molecules was found to be ~ 1050 K. Finally our value of the melting temperature, obtained in a totally unbiased manner [35], is in essentially perfect agreement with $T_m = 1064 \pm 14$ K independently obtained by thermodynamic integration by Frenkel's group [36].

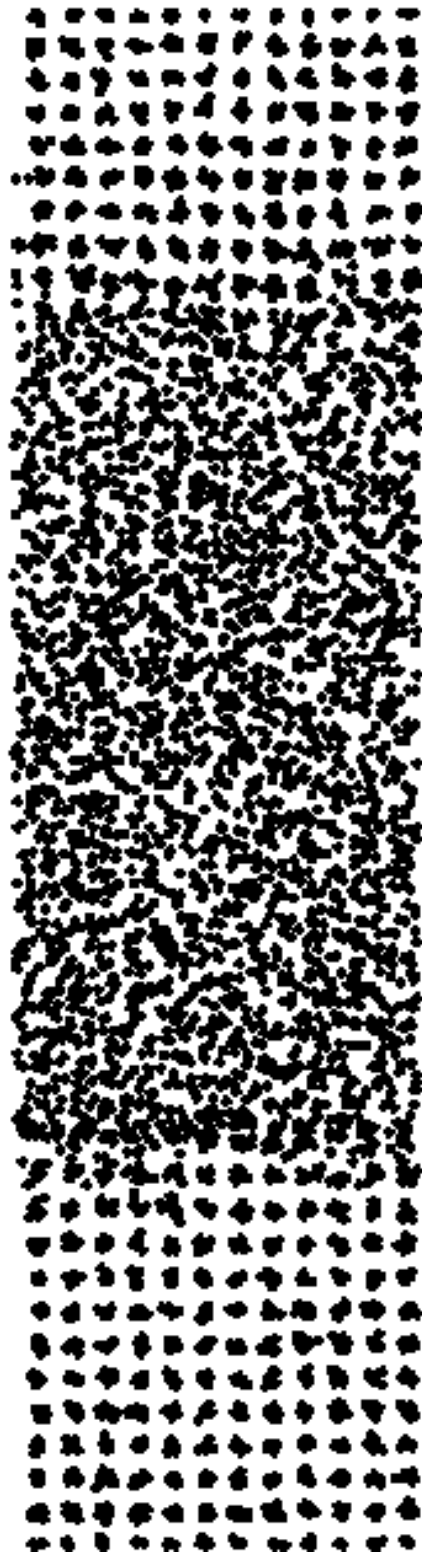


FIG. 8: Simulated coexistence of bulk solid and liquid. Periodic boundary conditions on all sides.

	Simulation	Experiment
T_m (K)	1066 ± 20	1074
ΔV	27%	26%
L (eV/molecule)	0.29	0.29
ΔS_m (k_B)	6.32	6.38
dP/dT (kbar/K)	0.0311	0.0357 [37]
α (10^{-6} K^{-1})	40.5	38.3
RMSD (\AA)	0.60	0.49
δ	20–24%	17–20% [23]

TABLE II: High temperature properties of NaCl. T_m is the melting temperature; ΔV is the volume jump at the melting point; L is the latent heat of melting; ΔS_m is the entropy variation at the melting point; dP/dT is the resulting Clausius-Clapeyron ratio at the melting point. α is the linear thermal expansion coefficient; RMSD is the root mean square displacement of atoms in the bulk solid at the melting point; δ is the RMSD over the Na-Cl distance, for the Lindemann melting criterion.

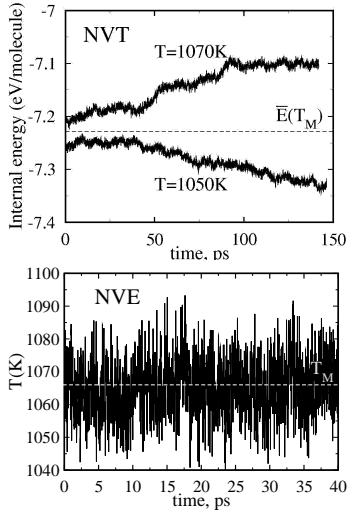


FIG. 9: (a) Canonical evolution of the internal energy at liquid-solid coexistence. The decrease of internal energy at $T = 1050$ K indicates that the SL interface moves toward recrystallization. Conversely, the increase of internal energy at $T = 1070$ K indicates that the liquid phase grows at the expenses of the solid phase. The internal energy for the BMHFT melting point of bulk NaCl lies in between. (b) Final microcanonical run showing the exact location of the melting temperature.

The latent heat (enthalpy of melting) is estimated as the change of the internal energy at T_m and found to be 0.29 eV/molecule. The calculated entropy jump at melting is thus $\Delta S_m = L/T_m = 6.32 \pm 0.1 k_B/\text{molecule}$. A slope of the melting line (Clausius-Clapeyron relation) $\frac{dP}{dT} = \frac{L}{T_m(v_l - v_s)}$ of 0.0311 kbar/K is then obtained. All these calculated results are in quite good agreement with experimental data. Tab. II summarizes the calculated values and their comparison with experiment.

IV. CRYSTALLINE NaCl(100): A NON-MELTING ANHARMONIC SURFACE

Satisfied with the above description obtained for bulk NaCl, we moved on to study the NaCl surfaces, by simulating slabs as described earlier. In slab simulations, we found the defect free NaCl(100) to warm up uneventfully, and to remain solid and totally dry up to T_m . The root mean square displacements (RMSD) of the first layer Na^+ and Cl^- ions at T_m were extracted and are shown in Fig. 10 and Fig. 11.

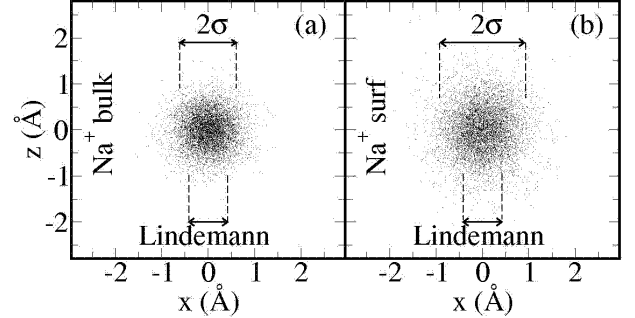


FIG. 10: Solid NaCl instantaneous displacements of Na^+ ions in (a) bulk and (b) first surface layer at T_m .

Unsurprisingly, the surface ions vibrate more than bulk ions. The ratio of surface/bulk RMSD at T_m is here 1.5. For comparison, in the Pietronero-Tosatti model [38] the critical surface melting value of this ratio is ~ 1.6 . Moreover, vibrations are somewhat more extended in direction perpendicular to the surface than in the in-plane direction.

We subsequently verified that even *above* T_m the NaCl(100) surface remained crystalline in a metastable state for at least 200 ps. In this overheated surface regime, solid NaCl(100) was found to possess a thick nucleation barrier against melting up to about $T^* = 1115$ K $\sim T_m + 50$ K, in the following sense. When a thin surface film consisting of l atomic layers was artificially melted,

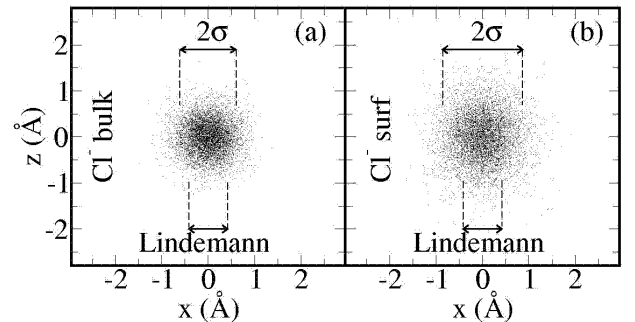


FIG. 11: Solid NaCl instantaneous displacements of Cl^- ions in (a) bulk and (b) first surface layer at T_m .

and then let evolve to equilibrium at a grid of temperatures $T \geq T_m$, the melted film was seen to spontaneously recrystallize for $l \leq l_{crit}(T)$, with $l_{crit}(T) \geq 1$ for $T \leq T^*$. (See Fig.12). That indicates that in this temperature range the overheated solid slab is locally stable, with a free energy barrier against overall melting [6].

Above T^* , overheating of crystalline NaCl(100) persisted until a higher “surface spinodal temperature” $T_{ss} \simeq 1215 \text{ K} \simeq T_m + 150 \text{ K}$, now however with only a thin nucleation barrier $l_{crit}(T)$ of a monolayer.

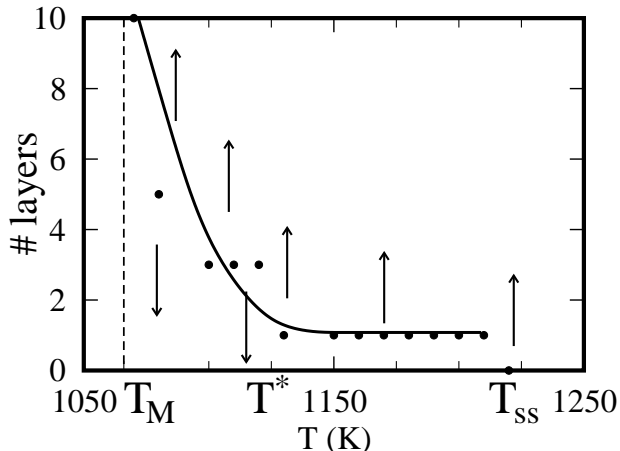


FIG. 12: Critical liquid film thickness vs. temperature for metastable solid NaCl(100) above T_m . This corresponds to the effective thickness of the free energy barrier for the nucleation of the NaCl melt at the solid surface.

Only at T_{ss} , as high as 150 K above T_m , does solid NaCl(100) become locally unstable and melt spontaneously. We find the pronounced metastability of this solid surface to persist at least up to T^* , or $\sim 50 \text{ K}$ above T_m even in presence of common surface defects, such as molecular vacancies or steps.

We have thus characterized NaCl(100) as a clear case of surface non-melting. This is a prediction that deserves to be tested in experiment. For a short enough time, it should be possible to raise the temperature of NaCl(100) by at least 50 K above T_m , without any liquid spontaneously nucleating at the surface. Of course, the solid surface will sublime very strongly at these temperatures. The experimental equilibrium vapor pressure of NaCl at T_m is 0.345 mmHg, a large value. As a consequence, surface vacancies will form and surface steps will flow due to evaporation (and to re-condensation when working at solid-vapor equilibrium). We note that the time scale for this kind of surface evolution is a much slower one than that addressed here. The experimental rate of evaporation found from empirical expression [39] valid for a variety of materials is about $4 \cdot 10^{-5} \text{ gr/cm}^2 \text{ s}$. For our typical 10×10 sized surface (200 surface NaCl units) of area around 3500 \AA^2 , and using an experimental vapor pressure of 0.345 mmHg the evaporation rate is $\sim 1.7 \cdot 10^5 \text{ s}^{-1}$. This indicates a typical evaporation time many orders of magnitude larger than our typical simulation

time.

That explains why in practice we never even observed in simulation a spontaneous evaporation event off the solid surface. This however does not invalidate the significance of the simulation results. At any given instant of a realistically long time evolution of NaCl(100), there will be of course molecular evaporation and step flow, but that will still leave defect free terraces much larger on average than those we simulated. These terraces will be fully crystalline even well above T_m , displaying precisely the microscopic non-melting behavior described above.

These considerations however suggest that surface non-melting in alkali halides could not easily be pursued with static or nearly static experimental probes, because sublimation and condensation will influence and possibly spoil the outcome. Perhaps the fast laser tools already employed for metals [40] could be brought to bear on this case too. The high vapor pressure also suggests techniques that do not rely on ultra-high vacuum [41]. We are currently considering in addition hard tip sliding friction as a tool, with results to be described in forthcoming paper.

V. SOLID SURFACE FREE ENERGY: THERMODYNAMIC INTEGRATION

In order to prepare for our thermodynamical assessment of the wetting of NaCl(100) by liquid NaCl, we eventually need to know according to eq. (2) the solid-vapor interface free energy γ_{sv} at the melting point.

We calculated γ_{sv} through thermodynamic integration [42] using the following relation:

$$\left(\frac{\partial(F/T)}{\partial(1/T)} \right)_{N,V} = E, \quad (11)$$

where F is the free energy and E the internal energy. We simulated for this purpose a 2880 molecule bulk system and independently a slab comprising 1440 molecules and an equivalent volume of vacuum. We kept in this manner the all-important Ewald sum convergence unchanged, (we judge the implied extra error due to size effects to be negligible by comparison). By integrating the internal energy over $(1/T)$ up to temperature T we separately obtained the bulk and the slab free energies per molecule up to T_s and to T_{ss} respectively. We did not explicitly include quantum freezing effects at low temperatures, because they represent a small correction in comparison with large thermal effects at the melting point. Nevertheless since quantum freezing takes place at temperatures $T \lesssim (1/4)\theta_D$, (θ_D is the Debye temperature), we started integration at $T_i = (1/4)\theta_D$ which is $\simeq 50 \text{ K}$ for NaCl, therefore using the $T = 50 \text{ K}$ state as a reference.

$$\frac{F(T)}{T} - \frac{F(T_i)}{T_i} = \int_{1/T_i}^{1/T} E(T') d\left(\frac{1}{T'}\right). \quad (12)$$

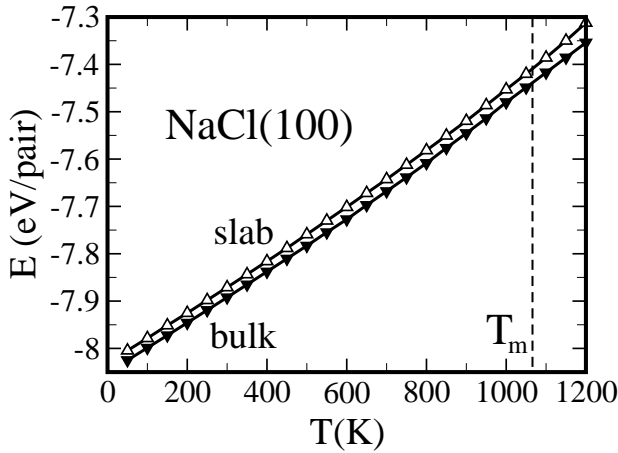


FIG. 13: Bulk (filled triangles) and slab (empty triangles) internal energies as a function of temperature. The slab consisted of 1440 NaCl molecules.

The bulk and slab internal energies as a function of temperature, are shown in Fig. 13. After integration, the difference between slab and bulk free energies per unit surface area (accounting the presence of two surfaces) equals the surface energy.

The NaCl(100) surface free energy calculated in this manner is displayed in Fig. 14. Starting at low temperature, we note from the start a low surface energy, reflecting the excellent charge order of this surface. Upon increasing temperature, there is an important thermal drop of the surface free energy, especially fast for $T \gtrsim 600$ K, indicating considerable additional anharmonicity of the solid surface relative to bulk solid NaCl. A good question is what part of that anharmonicity can be ascribed to temperature-dependent effectively harmonic vibrations, and what cannot.

To judge on that, we computed separately the bulk and slab vibrational spectra as a function of temperature. Using simulation trajectories in a bulk and in a slab comprising exactly the same number of molecules, we extracted the Fourier transformed velocity autocorrelation functions of ions $V_{\text{Na}}(\omega)$ and $V_{\text{Cl}}(\omega)$. The vibrational spectra are obtained as:

$$A(\omega) = \frac{m_{\text{Na}}}{k_B T} V_{\text{Na}}(\omega) + \frac{m_{\text{Cl}}}{k_B T} V_{\text{Cl}}(\omega). \quad (13)$$

By treating both the bulk and the slab spectra as a collection of harmonic oscillators, we obtained an effective surface vibrational free energy by subtracting their respective harmonic free energies off one another, and dividing the outcome by two, for two surfaces.

For increasing temperatures, the surface component of the slab spectra displays a stronger anharmonic softening than the bulk. This as anticipated gives rise to an “effective harmonic” drop of surface free energy, as shown by dots in Fig. 14. We conclude that whereas about half the total anharmonic free energy decrease can be ascribed to

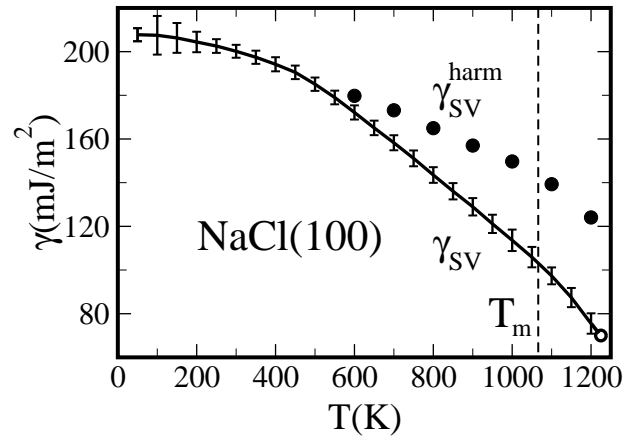


FIG. 14: The solid surface free energy from thermodynamic integration (line) and from the effective harmonic approximation (dots).

the effective surface vibrational free energy and in particular to the surface frequency softening with temperature, the remaining half cannot be accounted for in this way, representing “hard” anharmonicity.

In conclusion the surface free energy of NaCl(100) approximately halves its value from ~ 206 mJ/m² at 50 K to ~ 100 mJ/m² at T_m . Such a large decrease of the already unusually small low- T surface energy results in an exceptionally stable solid surface. While the physical reason for a low surface energy at low- T is clearly the perfect charge ordering, that for its large thermal decrease is the ability of rocksalt and of its surface to sustain exceptionally large anharmonic vibrations without loss of mechanical stability.

VI. THE LIQUID NaCl SURFACE

We proceeded next to study the liquid NaCl surface, or more correctly the liquid-vapor interface. There are earlier simulations of this liquid surface in the BMHFT model, notably by Heyes [16], and there is theory work in the Restrictive Primitive Model [43, 44]. The more sophisticated recent studies of Aguado et al. [17] of the liquid KI surface emphasize the role of polarization forces, and also summarize earlier work.

Notwithstanding that, our scope here is to pursue a homogeneous comprehensive study of all surface properties in a single simple model, and we therefore carried out a fresh study of NaCl in the BMHFT model, now with a larger size scale than that of Heyes [16].

Starting with the same $6 \times 6 \times 12$ solid slab used in the previous section for the study of NaCl(100), temperature was raised above the surface spinodal temperature causing the slab to melt. Subsequently, the liquid slab was gradually cooled down to T_m , and equilibrated for about 50 ps, after which correlations were examined.

Here too, evaporation of molecules and molecular dimers was very seldom observed, as an extremely rare event in our liquid surface simulations. The occasionally evaporated molecule traveled in vacuum to recondense within a relatively short time, but had no chance to get otherwise equilibrated during the flight. The occasional molecular evaporation or condensation events were very quickly “forgotten” in the chaotic liquid surface dynamics. In this regime they therefore do not appear to affect at all the overall liquid surface behavior. This allows us to neglect our lack of an evaporation/condensation statistics, in that its inclusion would not alter the liquid surface properties to be extracted by the simulation.

Because of the strong charge correlations in the bulk liquid, one might naively but not unreasonably have expected this liquid surface to be structured, maybe layered as in the metals [2], perhaps displaying a surface dipole [44]. The actual liquid local surface density profile $\rho_{+-}(z)$ obtained for both ionic species is shown in Fig. 15. All profiles are remarkably coincident and smooth, thus – as one could also see from earlier MD studies [16, 17] – totally devoid of layering. Moreover the Na and Cl profiles are superposable with very great accuracy, thus the liquid surface displays no static average dipole either, whereas the local time and space dependent dipole fluctuations are large.

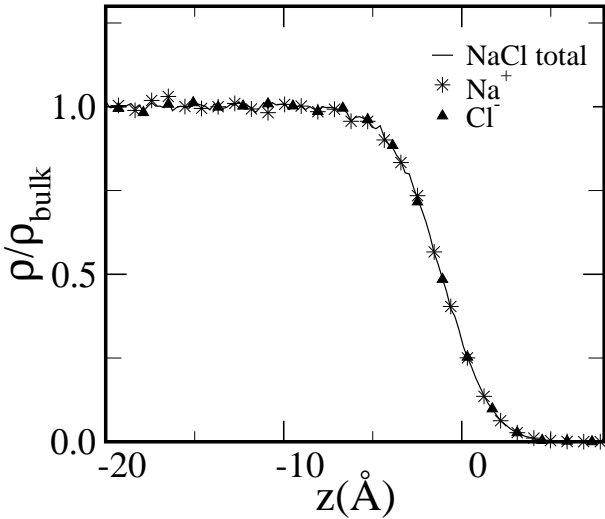


FIG. 15: Na, Cl and total density profiles of the simulated liquid surface of NaCl at $T = T_m$. Layering oscillations and surface dipoles are absent. Capillary fluctuations are very modest for our small cell size, and the large width of the liquid-vapor interface is a genuine local property of the surface.

We worried that the large apparent surface spatial width should really represent the local liquid surface structure, and not, *e.g.*, simply reflects long wavelength capillary fluctuations. For that purpose we carried out additional liquid slab simulations with alternatively a much smaller cell of size $4 \times 4 \times 4$, or a much larger one of size $10 \times 10 \times 15$. We found that the resulting surface

density profiles remain essentially the same. We conclude that the additional capillary broadening of the surface profile will only show up (logarithmically) for much larger sizes, and that the observed surface diffuseness is indeed intrinsic.

The nature of diffuseness of the NaCl liquid surface is clarified by the simulation snapshot of Fig. 16a, showing very pronounced local thermal fluctuations in the instantaneous surface profile. This picture, suggestive of a low surface tension, high entropy surface, is in apparent contradiction with the massive non-wetting of solid NaCl(100) by its own melt, the latter implying a relatively high liquid surface tension.

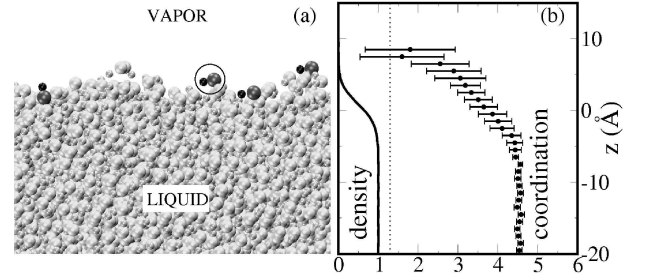


FIG. 16: a) Simulation snapshot of the NaCl liquid surface at T_m . Note the large thermal fluctuations, with some nearly molecular configurations highlighted in the outermost region; b) Coordination number $N(Z)$ and density profile, confirming a very smooth crossover from liquid ($N=4.6$) to molecular vapor ($N=1.3$ dotted line).

In order to clarify the situation, we undertook a direct calculation of the surface free energy γ_{LV} , equal to the surface tension, of liquid NaCl. The calculation was done by evaluating surface stress of the slab (which has two equivalent surfaces) via the Kirkwood-Buff formula:

$$\begin{aligned} \gamma_{LV} &= \frac{1}{2} \int_0^{L_z} dZ [\sigma_{\parallel}(Z) - \sigma_{\perp}(Z)] \\ &= -\frac{1}{8} \int_{-\infty}^{\infty} dZ \int d^3\mathbf{r}_{ij} \sum_{\alpha,\beta} \frac{x_{ij}^2 + y_{ij}^2 - 2z_{ij}^2}{r_{ij}} [\delta_{\alpha\beta} + \\ &\quad + \lambda(1 - \delta_{\alpha\beta})] f_{\alpha\beta}(r_{ij}) g_{\alpha\beta}^{(2)}(\mathbf{r}_{ij}; Z) \rho_{\alpha}(Z) \rho_{\beta}(Z) \\ &= -\frac{1}{8L_x L_y} \langle \sum_{i\alpha, j\beta} \frac{x_{ij}^2 + y_{ij}^2 - 2z_{ij}^2}{r_{ij}} [\delta_{\alpha\beta} + \\ &\quad + \lambda(1 - \delta_{\alpha\beta})] f_{\alpha\beta}(r_{ij}) \rangle \end{aligned} \quad (14)$$

where: $(\alpha, \beta) = (+, -)$, $i\alpha$ and $j\beta$ denote ions at site i or j , Z is the distance normal to the interface, L_x, L_y are the (x, y) dimensions of the supercell and $\sigma_{\parallel} = \frac{1}{2}(\sigma_{xx} + \sigma_{yy})$ and $\sigma_{\perp} = \sigma_{zz}$ are the tangential and normal components of the stress tensor respectively. Here $\langle \rangle$ denotes a canonical average and $\sum_{i\alpha, j\beta}$ is over all pairs of particles. Moreover $\mathbf{r}_{ij} = (x_{ij}, y_{ij}, z_{ij})$ is the interatomic distance, $f_{\alpha\beta}(r_{ij})$ is the force between atoms i and j , $g_{\alpha\beta}(\mathbf{r}_{ij}; Z)$ are the Na-Cl, Na-Na, Cl-Cl pair correlation

function measured in a slice centered at Z , $\rho_\alpha(Z)$ the average density of ion α near Z and finally λ is a parameter here equal to one, but inserted for later use.

The calculated liquid surface tension γ_{LV} is shown as a function of temperature in Fig. 20. The value at T_m is $104 \pm 8 \text{ mJ/m}^2$, in fairly good agreement with the experimental surface tension of 116 mJ/m^2 – and by chance essentially identical to that of the solid. A very large anharmonicity was shown earlier to explain the relatively low surface free energy of solid NaCl(100). The physical reasons that make the liquid surface tension so relatively high will be addressed below.

VII. LIQUID SURFACE ENTROPY DEFICIT: INCIPIENT MOLECULAR ORDER IN THE LIQUID SURFACE

We wish to understand the reasons for the relatively high surface free energy of liquid NaCl. A clue is provided by a comparison of solid and liquid surface excess entropies:

$$S_{\text{surf}} = -d\gamma/dT. \quad (15)$$

Generally, one would expect that the much looser structure and greater freedom of ionic motion at a liquid surface should yield a larger liquid surface entropy than that of the solid surface. Strikingly, in NaCl the smaller calculated temperature dependence of surface free energies shows just the reverse. We find a factor 2.6 lower surface entropy S_{LV} compared with S_{SV} of the solid surface. Let us focus on this inverted result, which indicates qualitatively speaking a liquid surface entropy deficit (SED). An entropy deficit is suggestive of some form of underlying surface short range order. The order is clearly not layering: so what is it instead?

The answer we found is that charge order, already very important in bulk, plays a newer and enhanced role at the molecular liquid surface. If surface thermal fluctuations are indeed very large, they are also revealingly *correlated*. For a Na^+ ion that instantaneously moves e.g., out of the surface, there is at least one accompanying Cl^- , also moving out; and vice versa. So while the large surface fluctuations smear the average liquid vapor density profile, bridging gently between the liquid and essentially zero in the vapor, (Fig. 15) the two-body correlations, described e.g. by the the Na-Cl pair correlation function $g_{+-}(\mathbf{r})$, and by its integral, the ion coordination number N , drop from values typical of the bulk liquid at T_m to the *nonzero* value of the molecular vapor. For a quantitative characterization, we calculated a locally defined charge coordination number:

$$N_{\pm}(Z) = \frac{1}{2\delta z} \int_{Z-\delta z}^{Z+\delta z} \left\{ dZ' \rho(Z') \int_{r < r_m} d^3\mathbf{r} g_{+-}(\mathbf{r}; Z') \right\} \quad (16)$$

where $r_m = 4.0 \text{ \AA}$ corresponds to the first local minimum of $g_{+-}(\mathbf{r})$, and δz is a small interval. Starting with Z

inside the liquid slab, where the environment is bulk-like, we recovered $N_{\pm L} = 4.6$ at T_m , as in the bulk liquid. Moving Z across the liquid-vapor interface we found $N_{\pm}(Z)$ to drop continuously from 4.6 downward (Fig. 16b).

In NaCl we know (even if simulation statistics is non-existing in the vapor) that $N_{\pm}(Z)$ for large Z is bounded below not by zero but by $N_{\pm v}$, the average value for the NaCl vapor at T_m . Experimentally the NaCl vapor consists for 69% of molecules ($N=1$), 31% of dimers, ($N=2$) and a trace of trimers [46]. The corresponding vapor average is $N_{\pm v} \simeq 1.3$. Here emerges the crucial difference between the molecular NaCl vapor and e.g., the atomic LJ vapor, where $N_{\pm v} \simeq 0$. The larger the coordination number of ions in the surface region, the less their configurational entropy, the higher the liquid surface tension. Hence incipient molecular order [45] could provide the reason for the SED found for liquid NaCl.

For a test of this idea, we repeated the same Kirkwood-Buff calculation of the surface tension done previously, now however by slightly and artificially altering in Eq. (14) the value of correlations g_{+-} at the surface. Specifically, we artificially reduced to zero the weight λ attributed to forces acting among Na^+ and Cl^- ions for that (extremely small) fraction of outermost surface atoms whose coordination number $N_{\pm} \lesssim N_{\pm v} \simeq 1.3$, the mean vapor value. The contribution of these configurations to the pressure should provide a good measure of the the influence of incipient molecular charge ordering to the surface free energy, in particular to the surface entropy. Through this highly artificial but in our view illuminating procedure, the surface internal energy (a mechanical variable) remains untouched, and thus only surface entropy is affected.

We first identified the *surface* Na and Cl atoms in the simulation by means of a simple algorithm. All ions are binned according to increasing Z and are represented by a sphere of finite radius (1.1 \AA in our case). An ion is considered a surface ion when the projection on the (x, y) plane of its representative sphere is non overlapping with that of any other ion at larger z . For each so identified surface ion i , we extracted from the simulation the instantaneous electrostatic potential value V_i , a quantity related to the coordination number, but more convenient to calculate and to handle. As shown in Fig. 17 the overall electrostatic potential distribution of, say, Na ions in the liquid slab is shifted toward the electrostatic potential value typical of the NaCl molecule, and away from that of the bulk liquid. This shift is evidently caused by the lower coordination of ions on the two surfaces of the slab, for the slab interior is bulk-like. The surface Na^+ ion potentials for example are shifted by $\sim 0.1 \text{ eV}$ on average relative to their bulk counterpart. The electrostatic potentials of Cl^- ions behave specularly, and are thus shifted by $\sim -0.1 \text{ eV}$ relative to their bulk counterparts.

As the next step we established the necessary connection between average electrostatic potentials (easily ex-

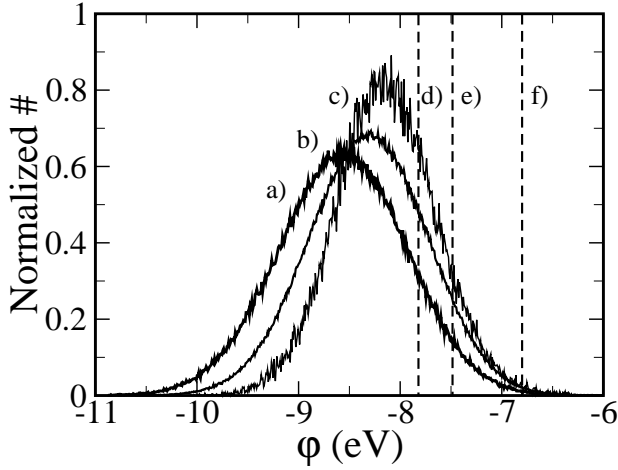


FIG. 17: The electrostatic potential distribution at Na^+ ions in (a) bulk liquid NaCl; (b) solid bulk, and (c) slab liquid of thickness 70 Å, at T_m . Comparison the potential at with BMHFT (d) trimers (e) dimers and (f) monomers is also provided. Precise values of the average ϕ are (a) -8.57 eV, (b) -8.32 eV, (c) -8.21 (d) -7.82 eV, (e) -7.485 eV, (f) -6.8 eV. The electrostatic distributions of Cl^- ions are just specular, that is identical to those of Na^+ , with a plus sign.

tracted from simulations, and at least in principle easily measurable) and coordination numbers (hard to extract from simulations, and probably harder to measure). The potential should vary monotonically with coordination, e.g., linearly for a fixed interatomic distance. Since in reality the Na-Cl distance increases with coordination, the overall dependence is somewhat less than linear as shown in Fig. 17. A raw histogram of electrostatic potentials against coordination numbers for the surface ions in the simulated liquid slab at T_m is shown in Fig. 18.

Finally, we computed a modified liquid surface tension by cutting off in the Kirkwood-Buff average in Eq. (14) the Coulomb part of the Na-Cl force contribution of surface Na ions, through a parameter λ of the form $\lambda = \theta(V_0 - V_i)$ where θ is the step function and V_0 is a cutoff potential value, selecting the type of correlations to be removed. For example, $V_0 = -6.8$ eV cuts off up to monomer correlations, $V_0 = -7.485$ eV cuts off up to dimer correlations, etc. In particular we choose $V_0 = -6.99$ eV, the value that cancels correlations for Na ions with $N \leq 1.3$, the vapor average.

With this tool, we are now able to examine more quantitatively the surface tension contribution due to the incipient surface molecular correlations causing $N_{\pm}(Z) \rightarrow N_{\pm v} \simeq 1.3$, by correspondingly choosing the cutoff potential $V_0 = -6.99$ eV. This modification generally affects an exceedingly small fraction of surface ions. In particular, the Na^- ions affected are quite few, as highlighted in Fig. 16a. Nevertheless the partial removal operated of the surface tension contribution due to this molecular part of surface Coulomb correlations yields a very considerable overall surface-tension decrease, with a large drop from $\gamma_{LV} = 104$ mJ/m² to $\gamma_{LV}^* = 53$ mJ/m²,

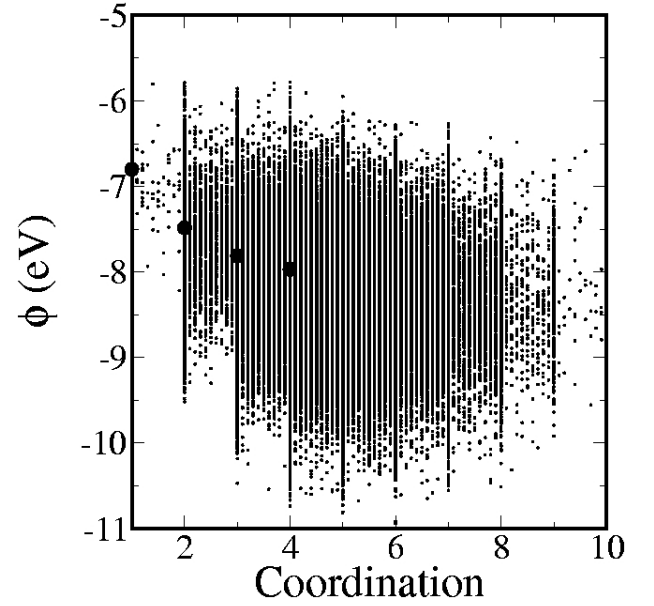


FIG. 18: Electrostatic potential distribution of surface Na^+ ions, plotted versus their own instantaneous coordination number. Superposed is the molecular correlation between potential and coordination (black dots).

as shown in Fig. 19, and Fig. 20. This we interpret as a

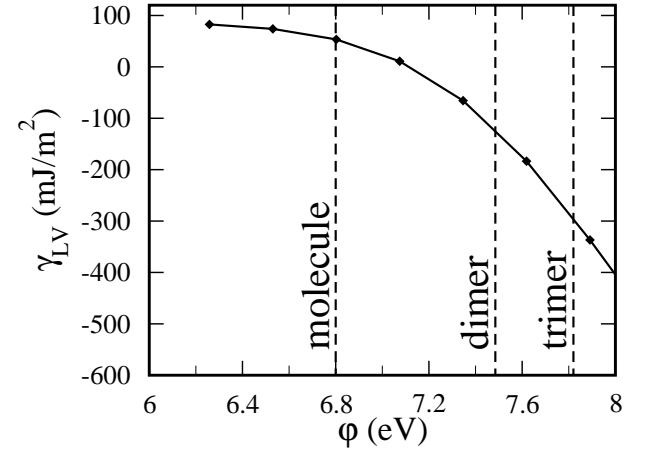


FIG. 19: The decrease of fictitious liquid surface tension γ_{LV}^* at T_m with increasing surface correlation coordination cutoff.

direct confirmation that incipient molecular surface correlations are indeed responsible for the liquid SED and for the resulting high surface tension. Remarkably, since now $\gamma_{LV}^* + \gamma_{SL} < \gamma_{SV}$, the surface tension drop following the hypothetical removal of short range surface molecular correlations would actually suffice to drive a *complete* instead of partial, wetting of NaCl(100) at the melting point.

The increased temperature slope $|d\gamma_{LV}^*/dT|$ confirms that the calculated surface tension drop is directly related to the restoring of a larger surface entropy, with re-

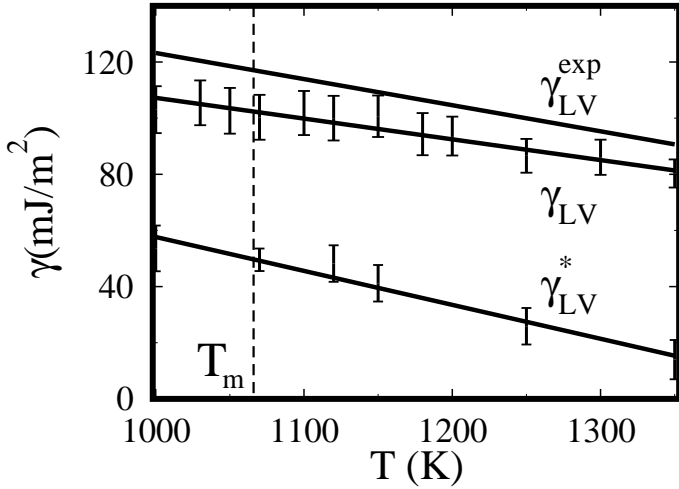


FIG. 20: Liquid NaCl surface tension. Note the good agreement of the calculated γ_{LV} with experiment γ_{LV}^{exp} . γ_{LV}^* : artificial surface tension calculated by setting $\lambda = 0$ for outer surface atoms with coordination below 1.3 (highlighted in Fig. 16a). Once surface molecular order is removed in this way, surface entropy rises, surface tension drops, as shown. Solid NaCl(100) would be completely wet by this artificial liquid.

removal of some of the SED through cancellation of molecular surface correlations. We found in fact that the drop from γ_{LV} to γ_{LV}^* at T_m corresponds exactly to the increased temperature slope $-d\gamma_{LV}^*/dT$, that is to the surface entropy increase, therefore with no change of surface internal energy as expected. In the presence of the surface molecular short-range order which we have just described, one could expect that the response to an external electric field should be strongly reduced due to the effective neutralization. Indeed this effect is present and very visible in Heyes' early simulations of a BMHFT liquid slab in a parallel electric field, which further confirms our interpretation [16].

VIII. SOLID-LIQUID INTERFACE FREE ENERGY: PARTIAL WETTING OF A NaCl DROPLET ON NaCl(100)

In the above Sections we calculated the SV and the LV surface free energies of NaCl. The intermediate solid-liquid (SL) interface free energy γ_{SL} , the third ingredient required to assess triple point wetting as in Eq. (1) is still missing. We calculated γ_{SL} through a simulation of the partial wetting of solid NaCl(100) by a droplet of melt, and by using Young's equation Eq. (3) that connects it to the partial wetting angle [47].

A 500 molecule NaCl cluster was initially melted to form a nanodroplet. The droplet and the solid slab were separately equilibrated at 1050 K, and then brought to contact (fig. 21a). During the first 100 ps after contact,

the droplet settled onto the substrate, slightly spreading and gradually approaching a final shape (fig. 21b). In the next 130 ps, spreading came to a halt, and the settled liquid droplet survived in a metastable, long lived state (Fig. 21c). At the end of the simulation, the droplet-substrate system were as depicted in Fig. 21d.

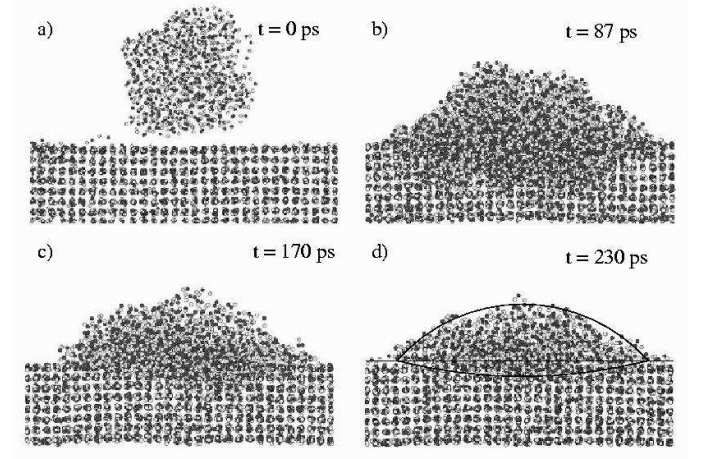


FIG. 21: Time evolution of the liquid NaCl drop on NaCl(100). Dark and light circles stand for the Na^+ and Cl^- ions respectively.

Let us consider the thermodynamics of this situation. Because we are below T_m (even if slightly) the true final equilibrium state should consist of a flat solid NaCl(100) surface, i.e. the nanodroplet should have completely spread and recrystallized. That however will take a very long time. While the nanodroplet still exists, it forms an external wetting angle θ_{LV} (Fig. 21), as well as an internal angle θ_{SL} . These angles obey the mechanical equilibrium equations Eq. (3) [9]. As it turns out, the angle θ_{SL} is irrelevant here, because it depends very critically on temperature. In particular close enough to T_m we expect $\theta_{SL} \simeq 0$ [9]. The external angle θ_{LV} is instead fully significant, as it depends very little on temperature, and indeed approximates the macroscopic wetting angle measured in the bubble experiment [13, 14].

To determine the external wetting angle θ_{LV} of the nanodroplet we analyzed 100 configurations in a 100 ps equilibrated run. The instantaneous atomic positions were plotted in cylindrical coordinates (r and z , where r is parallel to the surface), and from the profile of the drop, we determined the best approximation to a spherical segment, by determining the center position and the radius. The contact angle follows immediately by simple geometry from these two quantities. Our best estimate obtained slightly below T_m is $\theta_{LV} = 50^\circ \pm 5^\circ$. This value is in good agreement with the experimental value at the melting point (48°) [13]. At the end of the simulation the internal solid-liquid interface was still relatively sharp and flat, consistent with our assumption $\theta_{SL} \simeq 0$.

The connection between θ_{LV} and $\Delta\gamma_\infty = (\gamma_{LV} + \gamma_{SL}) -$

γ_{SV} is given directly by Young's equation:

$$\cos \theta_{LV} = 1 - \frac{\Delta\gamma_{\infty}}{\gamma_{LV}}. \quad (17)$$

When we plug in our calculated value of $\gamma_{SV} \simeq 103$ mJ/m², $\gamma_{LV} \simeq 104$ mJ/m² and finally $\theta = 50^\circ \pm 5^\circ$, we obtain $\gamma_{SL} = 36 \pm 6$ mJ/m² [48] and $\Delta\gamma_{\infty} = 37$ mJ/m².

A solid-liquid interface free energy of more than one-third the liquid surface tension is unusually large. Here, it is clearly attributable to an unusually large difference of density, as well as of correlations, between the solid and the liquid at the melting point. Corresponding to that, the solid-liquid interface is spatially rather abrupt, as shown by Fig. 21 and Fig. 8.

A further connection between $\Delta\gamma_{\infty}$ and the surface spinodal temperature T_{ss} was made by assuming a phenomenological SL-LV interface interaction of the form [10]:

$$\Delta\gamma_{\infty} \simeq \rho L a \left(\frac{T_{ss}}{T_m} - 1 \right). \quad (18)$$

With our value of $\Delta\gamma_{\infty}$, and $L = 4.813 \cdot 10^9$ erg/g, $a = 5.9$ Å we predict $T_{ss} = 1210$ K, quite close to that seen in simulations.

IX. DISCUSSION AND CONCLUSIONS

We studied in this paper the physics of the solid NaCl(100) surface and its wetting relationship with liquid NaCl at and near the melting temperature of bulk NaCl. Molecular dynamics simulations performed with classical BMHFT potentials were first of all shown to yield quite an accurate description of high temperature solid and liquid bulk. The NaCl(100) surface was subsequently studied, and found to be a non-melting surface, one that should in principle be possible to overheat well above T_m . The solid surface free energy was calculated by thermodynamic integration and seen to drop very considerably at high temperature due to large anharmonicities. The liquid NaCl surface was also studied, and found to be very diffuse, strongly fluctuating, and devoid of static structure such as layering, or surface dipoles. However, calculation of the liquid surface tension still gave a relatively large value, similar to the solid surface free energy at the melting point. The high surface tension signifies an unusual liquid surface entropy deficit, here ascribed to short range molecular order. In addition,

the solid liquid interface free energy was also found to be relatively large, about one third the liquid surface tension, consistent with the large density difference between solid and liquid. Direct simulation of a NaCl droplet deposited onto NaCl(100) demonstrated very realistically the incomplete wetting, implied by the clear satisfaction of Eq. (2). At T_m , we obtained the solid, liquid and solid-liquid surface free energies, 103 ± 4 , 104 ± 8 mJ/m², 36 ± 6 mJ/m² respectively, quantitatively explaining the surface nonmelting of NaCl(100) through Eq. (2). We note that nonwetting of solid KCl by its own liquid was argued earlier by J. Rose and S. Berry [49] based on the behavior of a (KCl)₃₂ clusters.

The present work is meant as a prototype study, ideally repeatable for other elemental and molecular systems including perhaps water and the surface of hexagonal ice [50].

In alkali halides, the extraordinarily poor wetting of the solid (100) surface by the melt is traced to the conspiracy of three separate factors, all of which can be finally related to the long range Coulomb interaction between ions: (i) surface anharmonicity stabilizes the solid surface; (ii) molecular correlations destabilize the liquid surface; (iii) a large density jump makes the solid-liquid interface very costly.

Several aspects uncovered in, or implied by, this study should be amenable to direct experimental verification. X-ray studies should confirm the diffuseness of the liquid surface, the abruptness of the solid-liquid interface, and the molecular short range order at the liquid surface. Overheating of solid NaCl(100) should be directly observable. So might the temporary settling of liquid mini-droplets. Moreover, the much larger solid surface entropy should cause the partial wetting angle of liquid on solid NaCl to *increase*, rather than decrease with temperature. A brief account of some of the present results has appeared in Ref.[51].

X. ACKNOWLEDGEMENTS

Work in SISSA/ICTP/Democritos was sponsored by MIUR FIRB RBAU017S8R004, FIRB RBAU01LX5H, and MIUR COFIN 2003, PRIN-COFIN2004, as well as by INFM (section F,G, "Iniziativa trasversale calcolo parallelo"). We acknowledge illuminating discussions with E. A. Jagla and A. C. Levi, and the early collaboration of W. Sekkal.

-
- [1] J. F. van der Veen, B. Pluis, and A. W. Denier van der Gon, in "Chemistry and Physics of Solid Surfaces VII", ed. by R. Vanselow and R. F. Howe, Springer, Heidelberg (1988).
 - [2] U. Tartaglino, T. Zykova-Timan, F. Ercolessi and E.

- Tosatti, Phys. Rep., **411**, 291(2005).
- [3] S. Dietrich, in "Phase Transitions and Critical Phenomena", ed. by C. Domb and J. Lebowitz, (Academic Press, London) Vol 12, p. 1 (1988),
- [4] This terminology also was suggested us by S.Dietrich.

- [5] S. G. J. Mochrie, D. M. Zehner, B. M. Ocko and D. Gibbs, Phys. Rev. Lett. **64**, 2925 (1990); H. M. van Pijsteren and J. W. M. Frenken, Surf. Sci. **275**, 383 (1992).
- [6] P. Carnevali, F. Ercolessi, and E. Tosatti, Phys. Rev. B **36**, 6701 (1987).
- [7] B. Pluis, A. W. Denier van der Gon, J. W. M. Frenken and J. F. van der Veen, Phys. Rev. Lett. **59**, 2678 (1987).
- [8] A. W. Denier van der Gon, R. J. Smith, J. M. Gay, D. J. O'Connor, and J. F. van der Veen, Surf. Sci. **227**, 143 (1990).
- [9] P. Nozières, J. Phys. (France) **50**, 2541 (1989).
- [10] F. D. Di Tolla, F. Ercolessi, and E. Tosatti, Phys. Rev. Lett. **74**, 3201 (1995).
- [11] A similar configuration is now predicted in NaCl by molecular dynamics simulation in Sec. VIII (see also Ref. [35]).
- [12] C. A. Croxton, *Statistical mechanics of the liquid surface*, Chichester, J. Wiley, 1980.
- [13] G. Grange and B. Mutaftschiev, Surf. Sci. **47**, 723 (1975).
- [14] L. Komunjer, D. Clausse and B. Mutaftschiev, J. Cryst. Growth **182**, 205 (1997).
- [15] H. M. van Pijsteren and J. W. M. Frenken, Europhys. Lett. **21**, 43 (1993).
- [16] D. M. Heyes, Phys. Rev. B **30**, 2182 (1984).
- [17] A. Aguado, M. Wilson, and P. A. Madden, J. Chem. Phys. **115**, 8603 (2001); A. Aguado, W. Scott, and P. A. Madden, J. Chem. Phys. **115**, 8612 (2001).
- [18] We estimate for NaCl(100) $H = (\pi/12) C_6(n_s - n_l)(n_l - n_v) = 0.00119$ eV See T. Zykova-Timan, U. Tartaglino, D. Ceresoli and E. Tosatti, to appear in: "Highlights in the quantum theory of condensed matter", a volume in honor of Mario Tosi, ed. Scuola Normale superiore di Pisa. (2005)
- [19] F. G. Fumi and M. P. Tosi, J. Phys. Chem. Solids **25**, 45 (1964).
- [20] A recent study by Aguado et al. [17] showed that polarization effects lower the liquid surface tension, bringing it in closer agreement with experiment for KI. In NaCl however, the experimental surface tension lies already above the rigid ion value.
- [21] I. Yeh and M. L. Berkowitz, J. Chem. Phys. **111**, 3155 (1999).
- [22] Landolt-Bornstein. Neue Serie. Gruppe III. v.7a: Kristallstrukturdaten anorganischer Verbindungen. Teil a: Schlusselemente F, Cl, Br, J(VII.Hauptgruppe) Halogenide und Halogenokomplexe./ Crystal structure data of inorganic compounds. Part a: Key elements F, Cl, Br, I(VII.main group) halides and complex halides, edited by K.-H. Hellwege and A. M. Hellwege (Berlin, Springer Verlag, 1973), Pt. A.
- [23] M. A. Viswamitra and K. Jayalakshmi, Acta Crystallogr. A **28**, S189 (1974).
- [24] J. R. Hardy and A. M. Karo, *The Lattice Dynamics and Statics of Alkali Halide Crystals*, New York, Plenum Press, 1979.
- [25] R. A. Cowley, W. Cochran, B. N. Brockhouse, and A. D. B. Woods, Phys. Rev. **131**, 1030 (1963).
- [26] M. J. L. Sangster and M. Dixon, Adv. Phys. **25**, 247 (1976).
- [27] P. Ballone, G. Pastore and M. P. Tosi, J. Chem. Phys. **81**, 3174 (1984).
- [28] G. Janz, *Molten salts handbook*, (New York, Academic Press, 1967).
- [29] J. E. Enderby and G. W. Neilson, Adv. Phys., **29**, 323 (1980).
- [30] M. Amini and R. W. Hockney, J. Non-Cryst. Solids, **31**, 447 (1979).
- [31] R. Young and J. P. O'Connell, Ind. Eng. Chem. Fundam. **10**, 418 (1971).
- [32] Strictly speaking the zero pressure melting temperature differs from the triple point temperature, which is slightly higher due to the finite triple point pressure. The triple point pressure is however only about $0.45 \cdot 10^{-6}$ kbar, which for $dP/dT \sim 0.03$ kbar/K yields extrapolated difference of only about 10^{-5} K between the the triple point temperature and the zero-pressure melting temperature, utterly negligible.
- [33] F. Ercolessi, O. Tomagnini, S. Iarlori and E. Tosatti, in *Nanosources and Manipulation of Atoms under High Fields and Temperatures: Applications* Vol. **235**, ed. by V. T. Binh, N. Garcia and K. Dransfeld (Kluwer, Dordrecht, 1993), p. 185.
- [34] A. R. Belonoshko, R. Ahuja, and B. Johansson, Phys. Rev. B **61**, 11928 (2000); J. R. Morris, C. Z. Wang, K. M. Ho, and C. T. Chan, Phys. Rev. B **49**, 3109 (1994).
- [35] T. Zykova-Timan, U. Tartaglino, D. Ceresoli, W. Sekkal-Zaoui and E. Tosatti, Surf. Sci. **566/568**, 794 (2004).
- [36] J. Anwar, D. Frenkel and M. G. Noro, J. Chem. Phys. **118**, 728 (2003).
- [37] J. Akella, S. N. Vaidya, and G. C. Kennedy, Phys. Rev. **185**, 1135 (1969).
- [38] L. Pietronero and E. Tosatti, Solid State Commun. **32**, 255 (1979).
- [39] S. Dushman *Scientific foundations of vacuum techniques*, (New York, Wiley & Sons, 1962).
- [40] J. W. Herman and H. E. Elsayed-Ali, Phys. Rev. Lett. **74**, 3201 (1995).
- [41] J. J. Métois and J. C. Heyraud, J. Phys. (France) **50**, 3175 (1989).
- [42] D. Frenkel and B. Smit, *Understanding molecular simulation: from algorithms to applications*, (San Diego, Academic Press, 2002).
- [43] B. Groh, R. Evans and S. Dietrich, Phys. Rev. E **57**, 6944 (1998); M. González-Melchor, J. Alejandro, and F. Bresme, Phys. Rev. Lett. **90**, 135506 (2003).
- [44] R. Evans and T. J. Sluckin, Molec. Phys. **40**, 413 (1980).
- [45] The role of charge neutrality in stabilizing the surface tension of molten salts was discussed earlier, notably by R. W. Pastor and J. Goodisman, J. Chem. Phys. **68**, 3654 (1978).
- [46] P. Davidovits and D. L. McFadden, *Alkali halide vapors: structure, spectra, and reaction dynamics*, (New York, Academic Press, 1979).
- [47] A preliminary account of partial wetting of NaCl(100) by a droplet of melt was presented in Ref [35].
- [48] After this paper was published we became aware of the work of C. Valeriani, E. Sanz and D. Frenkel, J. Chem. Phys. **122**, 194501 (2005). This highly relevant theory paper describes the homogeneous nucleation of a solid nucleus in mildly supercooled liquid "Tosi-Fumi" NaCl. From their calculated nucleation barrier they extract γ_{SL} larger or equal than 80 mJ/m^2 at a temperature between 800 and 825 K. This interfacial free energy is considerably larger than ours, namely $\gamma_{SL} = 36 \text{ mJ/m}^2$ at $T_m = 1066 \text{ K}$, calculated with a different method for exactly the same system. The reasons for this large difference are presently unclear. A decrease of γ_{SL} is actually reasonable, since the bulk properties of liquid and solid NaCl do get closer

as T rises. We also note that at $T=T_m$ the liquid surface tension γ_{LV} is as small as 104 mJ/m^2 (theory) or 116 mJ/m^2 (experiment) which makes $\gamma_{SL}=36 \text{ mJ/m}^2$ quite plausible there. It would be interesting to pursue this issue, and more generally the temperature evolution of γ_{SL} more explicitly in the future.

[49] J. P. Rose and R. S. Berry, J. Chem. Phys. **98**, 3246

(1993).

[50] V. F. Petrenko and R. W. Whitworth, *Physics of ice*, Oxford, University Press, 1999.

[51] T. Zykova-Timan, D. Ceresoli, U. Tartaglino and E. Tosatti, Phys. Rev. Lett. **94**, 176105 (2005).